The computation of convective heat transfer in rotating cavities

H. Iacovides
Mechanical Engineering Department, UMIST, Manchester, UK

J. W. Chew
Design Science Group, Rolls-Royce plc, Derby, UK

In this paper, numerical solutions of the Reynolds-averaged Navier–Stokes equations are presented for convective heat transfer inside axisymmetric rotating disc cavities. The study involves the examination of three different disc-cavity configurations and the use of four different mathematical models of turbulence. The three configurations are a rotating cavity with flow entering axially at the center and leaving radially through the outer shroud, a rotating cavity with central axial throughflow, and a rotor-stator system with axial flow injection through the stator center and outflow through the annulus formed between the rotor disc and the outer shroud. Of the four turbulence models, three are based on the zonal modeling approach with the k-ε model in the main flow region and alternative low-Reynolds number treatments across the near-wall regions. These near-wall alternatives consist of two versions of the mixing-length hypothesis and a one-equation k-transport model. The fourth turbulence model is the mixing-length hypothesis applied over the entire cavity. Comparisons with available heat transfer measurements show that none of the models is successful in all cases examined. Considering overall performance, the k-ε model with the one-equation near-wall treatment is preferred.

Keywords: rotating cavities; computation; heat transfer

1. Introduction

Use of computational fluid dynamics for estimating flow and heat transfer in the rotating disc cavities of gas turbine engines is becoming increasingly popular (see, for example, Roscoe et al. 1988; Subbaraman et al. 1990). A wide variety of cavity configurations occur, and experimental measurements at engine conditions are both difficult and costly. Thus, computational fluid dynamics offers an attractive method of extrapolating from a limited database to particular engine designs. In this paper, numerical solutions of the axisymmetric Reynolds-averaged Navier–Stokes and energy equations with various models of turbulence are compared with other workers' heat transfer measurements for flow in model disc cavities. The main objective is to clarify the capabilities and limitations of current predictive methods. A further objective is to clarify the interpretation of the measurements. Some areas where further work is needed, on both methods development and experimental research, are also identified.

A particular feature of the disc cavity flows is the thin boundary layers that form on the disc surfaces. These are often called Ekman or Ekman-type layers in recognition of Ekman's (1905) analytical solution for the laminar boundary layer formed on a rotating surface in a differentially rotating fluid. (This solution is derived by treating the flow as a small perturbation from rigid body rotation, but the terminology is sometimes used in conditions far from this.) If the disc rotates faster than the main flow, then fluid is pumped radially outwards in the boundary layer, and if the main flow rotates faster than the disc, then the boundary layer flow is radially inwards. In many situations the cavity flow is essentially controlled by the disc boundary layers. Examples include radial outflow between co-rotating discs as studied by Owen et al. (1985) and the enclosed rotating disc as studied by Daily and Nece (1960) and Daily et al. (1964).

As discussed more fully by Chew (1990), most attempts at developing predictive methods for disc cavity flows to date have concentrated on flows dominated by the disc boundary layers. It has now been demonstrated that various numerical solution schemes and turbulence models can be applied with some success to such flows. In a recent study, Iacovides and Theofanopoulos (1991) applied a zonal turbulence modeling approach to various disc cavity flows. In the main flow, either the k-ε eddy viscosity or an algebraic stress model (ASM) was applied. In the wall regions, two different mixing length models were employed. From comparisons with velocity measurements and other workers' calculations, it was concluded that the near-wall turbulence modeling was most important. Although no single model was considered fully satisfactory, the performance of various models might be considered adequate for many engineering calculations. These conclusions are consistent with earlier work using mixing length and low Reynolds number k-ε models for flow in similar cavities (e.g., Chew and Vaughan 1988; Morse 1987). Chang et al. (1990) have also found some agreement of the zonal model with measurements for co-rotating discs enclosed by a stationary shroud, a problem of particular relevance to computer disc storage systems.

Various workers have produced heat transfer predictions for disc cavity flows, but the data available for validation are more

Address reprint requests to Dr. Iacovides at the Mechanical Engineering Department, UMIST, P.O. Box 88, Manchester M60 1QD, UK.

Received 2 April 1992; accepted 10 July 1992

limited than those for flow measurements. One particularly useful experimental study is that of Northrop and Owen (1988). These workers' measurements for heat transfer from co-rotating discs with a radial outflow of fluid were found to be in reasonable agreement with predictions from an integral method (Chew and Rogers 1989). Comparisons with earlier experimental data were inconclusive due to experimental uncertainty. Agreement of Northrop and Owen's data with finite-difference calculations employing turbulence models has been demonstrated by Ong and Owen (1989) and Morse and Ong (1990). Ong and Owen used a mixing-length model with boundary-layer assumptions, whereas Morse and Ong used a low Reynolds number k-ε model in a recirculating flow solver.

Three different disc cavity configurations are considered in the present study and these are illustrated in Figure 1. Case (i) models Northrop and Owen's experiment with flow entering a rotating cavity axially at the center and leaving through a slot in the cylindrical shroud. This slot provided an axisymmetric model of the experiment in which flow left the cavity through a number of discrete holes. Case (ii), a rotating cavity with a central axial throughflow, has been studied experimentally by Farthing et al. (1990a, 1990b). Although it is known that the flow in this case may be unsteady and three-dimensional (3-D), there are limiting conditions for which the axisymmetric and steady assumptions used here might be expected to apply. The third example involved a rotating disc facing a stationary disc through which a narrow central jet of air entered the cavity and impinged on the rotor. This models the experiments of Bunker et al. (1990a, 1990b), although their angled shroud has been replaced with a cylindrical shroud for computational convenience. In this example, the jet impingement is expected to dominate over rotational effects over the inner part of the cavity.

Four different effective viscosity turbulence models are compared in this study. These include three zonal models, all using the k-ε model in the main flow but with two different mixing-length near-wall treatments (as in Iacovides and Theofanopoulos) and a one-equation (k-l) near-wall treatment. The fourth model employs the mixing-length hypothesis

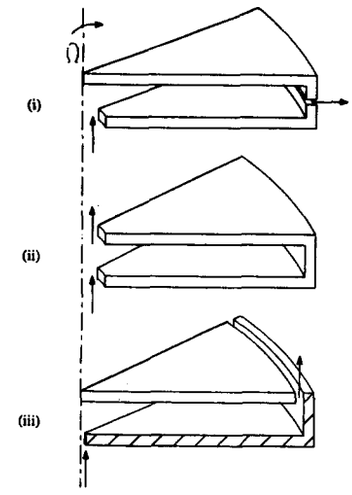

Figure 1 The three configurations studied

throughout the flow field and is similar to models that have been used with success for various rotating disc and cone problems (Koosinlin et al. 1974; Chew 1985; Chew and Vaughan 1988). Details of the models and the numerical solution are given in the next section. Results for the three test configurations are then presented and discussed in the following sections. The main conclusions, including a summary of the performance of the different turbulence models, are given in the final section.

2. Mathematical Modeling

An axisymmetric cylindrical coordinate system is employed. The axial, radial, and circumferential directions are denoted by x, r, and θ, respectively. The corresponding velocity components are U, V, and W.

Notation

a	Inlet radius
b	Cavity radius
C_w	Mass flow parameter $= \dot{m}/\mu b$
C_ε, $C_{\varepsilon 2}$, C_μ	Turbulence model constants
D	Damping function in turbulence model, section 2.4
G	Turbulence energy production term, section 2.2
k	Turbulence energy
l_m, l_ε, l_μ	Turbulence length scales, sections 2.3 and 2.4
$\dot{m}$	Net mass throughflow rate
p	Static pressure
P_k	Turbulence energy production term, section 2.2
Pr	Prandtl number
q	Heat flux
r	Radial coordinate
r_o	Outer radius of rotating disc
Re_z	Axial flow Reynolds number
Re_ϕ	Rotational Reynolds number
s	Axial width of cavity
t	Width of exit for rotor-stator example
T	Temperature
U, V, W	Axial, radial, and tangential velocity components
U_T	Friction velocity, section 2.4
x	Axial coordinate
y^+	Nondimensional wall distance YU_T/ν
y^*	Nondimensional wall distance $= Yk^{1/2}/\nu$
Y	Distance from wall

Greek symbols

ε	Turbulence energy dissipation rate or $U_{in}/\Omega a$ in Figure 4
θ	Angular coordinate
μ	Dynamic viscosity
μ_e	Effective viscosity $\mu_T + \mu$
μ_T	Turbulent viscosity
ν	Kinematic viscosity $= \mu/\rho$
ρ	Density
σ_T, σ_k, σ_e	Turbulent Prandtl or Schmidt numbers
Ω	Angular velocity

Subscripts

av	averaged over disc surface
in or I	at inlet conditions
s	surface value

2.1. Mean flow equations

The equations of mean motion are as follows:

Continuity

$$\frac{1}{r}\left\{\frac{\partial}{\partial x}(\rho r U)+\frac{\partial}{\partial r}(\rho r V)\right\}=0$$

U-momentum

$$\frac{1}{r}\left\{\frac{\partial}{\partial x}(\rho r U^2)+\frac{\partial}{\partial r}(\rho r V U)\right\}=-\frac{\partial p}{\partial x}+\frac{1}{r}\left\{2\frac{\partial}{\partial x}\left[r\mu_e\left(\frac{\partial U}{\partial x}\right)\right]+\frac{\partial}{\partial r}\left[r\mu_e\left(\frac{\partial U}{\partial r}+\frac{\partial V}{\partial x}\right)\right]\right\}$$

V-momentum

$$\frac{1}{r}\left\{\frac{\partial}{\partial x}(\rho r U V)+\frac{\partial}{\partial r}(\rho r V^2)\right\}=-\frac{\partial p}{\partial r}+\frac{1}{r}\left\{\frac{\partial}{\partial x}\left[r\mu_e\left(\frac{\partial V}{\partial x}+\frac{\partial U}{\partial r}\right)\right]+2\frac{\partial}{\partial r}\left[r\mu_e\left(\frac{\partial V}{\partial r}\right)\right]\right\}+\rho\frac{W^2}{r}-2\frac{\mu_e V}{r^2}$$

W-momentum

$$\frac{1}{r}\left\{\frac{\partial}{\partial x}(\rho r U W)+\frac{\partial}{\partial r}(\rho r V W)\right\}=\frac{1}{r}\left\{\frac{\partial}{\partial x}\left(r\mu_e\frac{\partial W}{\partial x}\right)+\frac{\partial}{\partial r}\left(r\mu_e\frac{\partial W}{\partial r}\right)\right\}-\rho\frac{VW}{r}-\frac{\partial}{\partial r}\left(\mu_e\frac{W}{r}\right)$$

where μ_e is the effective viscosity defined as $\mu_e=\mu+\mu_T$, ρ is density, and p is static pressure. In these equations the effects of compressibility in the viscous terms are neglected.

Energy equation

$$\frac{1}{r}\left\{\frac{\partial}{\partial x}(\rho r U T)+\frac{\partial}{\partial r}(\rho r V T)\right\}=\frac{1}{r}\left\{\frac{\partial}{\partial x}\left[r\left(\frac{\mu}{\mathrm{Pr}}+\frac{\mu_T}{\sigma_T}\right)\frac{\partial T}{\partial x}\right]+\frac{\partial}{\partial r}\left[r\left(\frac{\mu}{\mathrm{Pr}}+\frac{\mu_T}{\sigma_T}\right)\frac{\partial T}{\partial r}\right]\right\}$$

Pr is the molecular Prandtl number and σ_T the turbulent Prandtl number. The value of σ_T is assumed to be constant at 0.9. For air, the value of 0.71 is used for the molecular Prandtl number. Frictional heating has been neglected in the energy equation. Although this assumption is not appropriate at engine-running conditions, it is reasonable for the conditions considered below.

2.2. k-ε model

The following equations are used in the three zonal models for the flow outside the near-wall region:

k-Transport

$$\frac{1}{r}\left\{\frac{\partial}{\partial x}(\rho r U k)+\frac{\partial}{\partial x}(\rho r V k)\right\}=\frac{1}{r}\left\{\frac{\partial}{\partial x}\left[r\left(\mu+\frac{\mu_T}{\sigma_k}\right)\frac{\partial k}{\partial x}\right]+\frac{\partial}{\partial r}\left[r\left(\mu+\frac{\mu_T}{\sigma_k}\right)\frac{\partial k}{\partial r}\right]\right\}+P_k-\rho\varepsilon$$

ε-transport

$$\frac{1}{r}\left\{\frac{\partial}{\partial x}(\rho r U\varepsilon)+\frac{\partial}{\partial r}(\rho r V\varepsilon)\right\}=\frac{1}{r}\left\{\frac{\partial}{\partial x}\left[r\left(\mu+\frac{\mu_T}{\sigma_\varepsilon}\right)\frac{\partial\varepsilon}{\partial x}\right]+\frac{\partial}{\partial r}\left[r\left(\mu+\frac{\mu_T}{\sigma_\varepsilon}\right)\frac{\partial\varepsilon}{\partial r}\right]\right\}+C_{\varepsilon1}\frac{\varepsilon}{k}P_k-C_{\varepsilon2}\rho\frac{\varepsilon^2}{k}$$

where

$$\mu_T=C_\mu\rho k^2/\varepsilon \quad P_k=\mu_T G$$

and

$$G=2\left(\frac{\partial U}{\partial x}\right)^2+2\left(\frac{\partial V}{\partial r}\right)^2+2\left(\frac{V}{r}\right)^2+\left(\frac{\partial U}{\partial r}+\frac{\partial V}{\partial x}\right)^2+\left(\frac{\partial W}{\partial x}\right)^2+\left(\frac{\partial W}{\partial r}-\frac{W}{r}\right)^2$$

The constants that appear in the above equations have the following values:

C_μ	$C_{\varepsilon1}$	$C_{\varepsilon2}$	σ_k	σ_ε
0.09	1.44	1.92	1.00	1.30

At the interface with the near-wall models, patching conditions set k and ε to the values given by the near-wall model, as described below.

2.3. One-equation model

The following equations are applied in the near-wall region for the k-ε/one-equation (k-ε/1-eqn) zonal model. They are based on Wolfshtein's (1969) proposal.

The k-transport equation is the same as the one in the k-ε model.

The dissipation rate ε is obtained from a prescribed length scale l_ε according to

$$\varepsilon=k^{3/2}/l_\varepsilon$$

where

$$l_\varepsilon=2.55\,Y[1-\exp(-0.263y^*)].$$

Y is the distance to the nearest wall from the point in question, and y^* is defined as

$$y^*=Yk^{1/2}/\nu$$

The turbulent viscosity, μ_T, is then obtained from

$$\mu_T=\rho C_\mu l_\mu k^{1/2}$$

where

$$l_\mu=2.55\,Y[1-\exp(-0.016y^*)].$$

2.4. Mixing-length model

In the mixing-length model, the turbulent viscosity is obtained from

$$\mu_T=\rho l_m^2\sqrt{G}$$

where $l_m=0.42\,Y[1-\exp(-D)]$ in the near-wall region.

In the van Driest (1956) version, used in the zonal model k-ε/ML1 and the full mixing-length model ML, D is defined as

$$D = YU_T/(26\nu)$$

where U_T is friction velocity defined as

$$U_T = \left(\frac{\tau_w}{\rho}\right)^{1/2}$$

In the Koosinlin et al. (1974) version, used in the zonal model k-ε/ML2,

$$D = YU_T(\tau/\tau_w)^{1.5}/(26\nu)$$

For the two zonal models, patching conditions to the k-ε model are given by the relations

$$\rho\varepsilon = P_k$$

$$k^{3/2} = l_m\varepsilon$$

For the full mixing-length model ML, l_m outside the near-wall region is given by

$$l_m = 0.085\delta$$

where δ is an estimate of the boundary-layer thickness. The edge of the near-wall region is chosen so that l_m is continuous. In this model a Richardson number correction is applied in the boundary layers on the cylindrical surfaces. Further details are given by Chew and Vaughan (1988).

3. Numerical aspects

Two different finite volume codes have been employed in these numerical investigations. The staggered grid approach is used in both codes, and the pressure field is obtained through use of the SIMPLE algorithm. The code used for the k-ε computations, within the zonal modeling approach, is described by Iacovides and Theofanopoulos (1991). Details of the code with which the mixing length computations were carried out can be found in Vaughan et al. (1989).

3.1. Boundary conditions

3.1.1. Rotating cavity with outflow. Along the disc walls ($x = 0$ and $x = s$) and also along the outer shroud ($r = b$), the axial and radial velocity components U and V are set to zero and the tangential velocity component to Ωr. At the central entrance hole ($x = 0$ and $0 < r < a$), the fluid is assumed to have uniform axial velocity $U_{in} = \dot{m}/\rho\pi a^2$ and swirls in solid-body rotation ($W = \Omega r$). Inlet turbulence energy levels were set to 0.0001 U_{in}^2 in the case of the k-ε computations. The inlet dissipation rate ε_{in} was subsequently set to $k_{in}^{3/2}/(0.68a)$. At the outer-shroud exit slot, different boundary conditions were used in the two codes. For the k-ε computations, a uniform radial pressure gradient is imposed across the exit boundary. The value of this exit boundary pressure difference is determined from overall continuity considerations, thus ensuring that the total flow rate across the exit boundary is equal to the inlet flow rate. For the mixing-length calculations, uniform radial velocity, zero axial velocity, and zero gradient of tangential velocity are assured. The fluid was assumed to enter the cavity with uniform temperature, and the temperature distribution along the disc walls was assumed to increase radially according to the measurements of Northrop and Owen (1988).

3.1.2. Rotating cavity with axial throughflow. Hydrodynamic and thermal boundary conditions at the cavity walls and also at the central entrance hole were set as described in section 3.1.1. At the central exit hole, a uniform axial pressure gradient was assumed, and its level was determined from overall continuity considerations.

3.1.3. Rotor-stator system with radial outflow. Along the surfaces of the stationary disc ($x = 0$) and of the outer shroud ($r = b$), all velocity components were set to zero. Across the central injection hole ($x = 0$, $r < a$) and also around the outer exit, ($x = s$, $b - t < r < b$) entry and exit conditions, respectively, were set in a similar manner to the previous two cases. Heat transfer predictions were carried out both with constant wall temperature and also with constant wall heat flux thermal boundary conditions.

3.2. Grid arrangement

Nonuniform grids consisting of up to 51 × 76 axial and radial nodes, respectively, have been employed in this study. For the case of the rotating cavity with outflow, computations performed with a 35 × 50 mesh indicate that numerical uncertainties have been kept down to acceptably low levels.

In computations using the zonal modeling approach, the simpler low-Reynolds number models are employed across the first ten near-wall nodes. The y^+ value along the nodes adjacent to the walls was around 1 and along the interface between the low- and high-Reynolds number regions between 60 and 100.

4. A rotating cavity with radial outflow

This configuration, shown in Figure 1(i), matches the experimental apparatus of Northrop and Owen (1988). The cavity outer radius, b, is 428 mm, and the inlet radius, a, and axial spacing, s, are given by $a/b = 0.104$ and $s/b = 0.138$. Computations were carried out for selected values of the rotational Reynolds number ($Re_\phi = \rho\Omega b^2/\mu$, where Ω is the angular velocity of the cavity) and mass flow parameter ($C_w = \dot{m}/\mu b$, where $\dot{m}$ is the net mass throughflow rate). Actual flow rates, as opposed to nominal C_w values given by Northrop and Owen and quoted here, and inlet and disc surface temperatures were obtained from the tabulated data of Northrop (1984). All the cases considered had a "positive temperature profile" in which temperature increases with radius over most of the disc. The outer, insulated shroud was treated as adiabatic. A uniform axial velocity and angular velocity Ω was assumed at the inlet, the experimental conditions being uncertain.

Figure 2 shows results obtained using the k-ε/1-eqn model for velocity vector plots and contours of tangential velocity in the r-z plane for two of the cases considered. These conditions represent extremes of the experimental range; in Case (1) the rotational speed is high ($Re_\phi = 3.1 \times 10^6$) and the throughflow rate is low ($C_w = 1{,}400$). In the first case the flow can be said to be rotationally dominated; the supplied flow is rapidly entrained into the disc boundary layers, which develop into Ekman layers separated by a rotating core in which the radial and axial velocities are zero. In Case (ii) the supplied flow is considerably greater than that needed to supply the disc pumping, and the effects of rotation are comparatively weak. The inlet flow impinges on the downstream disc, generating a wall jet and a recirculating zone that transports fluid radially inward along the opposing disc.

Heat transfer results, in the form of disc Nusselt-number distributions ($Nu = rq/k(T_s - T_i)$, where q is heat transfer from

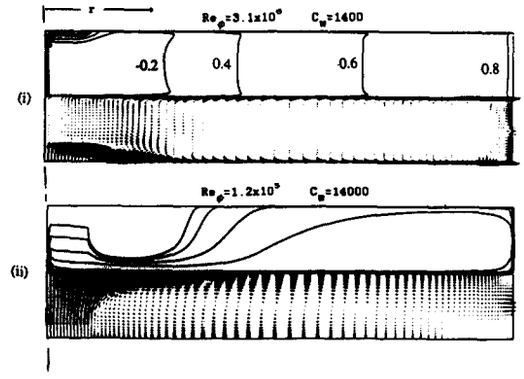

Figure 2 Velocity vectors and $W/\Omega r$ contour plots for a rotating cavity with radial outflow

the disc, T_s is surface temperature, and T_I is inlet temperature) are shown in Figure 3. Cases (ii) and (iii) correspond to the conditions in Figure 2 and Cases (i) and (iv) give results at other extremes of the experimental range; high flow (C_w = 14,000), high speed ($Re_\phi = 3.2 \times 10^6$), and low flow ($C_w$ = 1,400), low speed ($Re_\phi = 1.3 \times 10^5$). The two discs are designated upstream and downstream relative to the axial inlet flow. In addition to

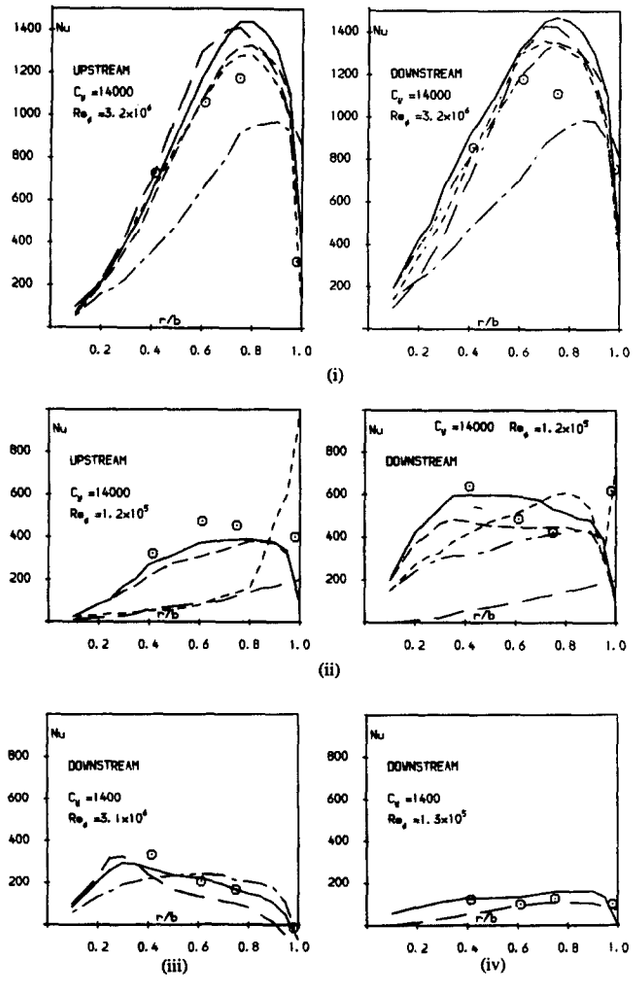

Figure 3 Nusselt number comparisons for a rotating cavity with radial outflow 0: Measurements, Northrop and Owen (1988) ———: k-ε/1-eqn; — — —: k- ε/ML1; — — —: k-ε/ML2; ------: ML; ——— ———: integral method

the present results using various turbulence models and Northrop and Owen's data from heat flux meters, the integral solution of Chew and Rogers (1988) is also shown. It is clear that while the performance of the integral solution is reasonable for Cases (i), (iii), and (iv), it does badly in Case (ii) for which the effects of rotation are relatively weak.

A comparison of the four different turbulence models for Cases (i) and (ii) is given in Figure 3. Looking first at Case (i), it is clear that the k-ε/ML2 model severely underpredicts the measurements. Of the other models, ML and k-ε/ML1 are apparently in best overall agreement with the measurements, while the k-ε/1-eqn model tends to overpredict the heat transfer. In Case (ii), the performance of the ML model for the upstream disc heat transfer is clearly inadequate. Of the other models, the k-ε/1-eqn model arguably gives the best overall performance for this instance. Note that the results from k-ε/ML2 for the upstream disc in Case (ii) were very close to those from the k-ε/ML1 model; they were omitted from the figure for clarity. Results for Case (iii) are consistent with Case (i) in that the k-ε/ML2 model underpredicts the peak Nusselt number (which occurs in the region of the point at which all the supplied flow is entrained into the disc boundary layers). However, the k-ε/1-eqn model does not overpredict the peak Nusselt number as in Case (i). Predictions from the k-ε/1-eqn model agree with the measurements to within experimental uncertainty for both Cases (iii) and (iv).

From the above results it is deduced that the k-ε/1-eqn model performs reasonably well for all the cases considered. The k-ε/ML2 and ML model have definite shortcomings in certain cases. For the two cases to which it was applied, the performance of the k-ε/ML1 model is comparable to the k-ε/1-eqn model. Considering these results and for consistency within the framework of transport-based turbulence modeling, the k-ε/1-eqn model was selected from the various two-layer models for further evaluation and investigations.

Ong and Morse (1990) presented a more complete comparison of predictions with Northrop and Owen's data using a slightly modified version of the Jones and Launder (1972) low Reynolds number k-ε model. Their agreement with data is comparable to, and arguably slightly better than, that of the k-ε/1-eqn model given above. However, it would be dangerous to base general conclusions on a specific test case, and low Reynolds number k-ε models have certain disadvantages such as requiring high near-wall resolution (see, for example, Rodi 1990; Yap 1987). For overall performance, the two-layer model might still be preferred.

5. A rotating cavity with axial throughflow

This geometry, shown in Figure 1(ii), was studied experimentally by Farthing et al. (1990a, 1990b) using the same basic apparatus as Northrop and Owen (1988). The outer radius of the cavity was 426 mm with an aspect ratio $s/b = 0.138$ and the inlet radius given by $a/b = 0.106$. The radius of the outlet is equal to that of the inlet. In the conditions considered here, both discs are heated with an "increasing temperature distribution," the maximum disc temperature being typically 80 K higher than the inlet air temperature. The outer shroud is insulated.

Before presenting the numerical results it is useful to discuss the measurements. Farthing et al. claim that their local Nusselt number data are reasonably represented by a correlation having similar form to that for laminar natural convection from a vertical plate, although substantial scatter of the data about this correlation is apparent. These authors also conclude that although the flow structure between the discs is strongly

influenced by Rossby number, there appears to be no consistent effect of this parameter on the magnitude of the local Nusselt numbers. In Figure 4, Farthing et al.'s data for the average Nusselt number ($Nu_{av} = q_{av}\, b/k(T_{s,av} - T_i)$, where q_{av} and $T_{s,av}$ are mean heat flux and temperature obtained by averaging over the disc area) have been replotted. The data are for different values of the axial Reynolds number ($Re_z = 2\,\rho U_{in} a/\mu$, where U_{in} is the average axial velocity at inlet) and for values of Re_ϕ ranging from 1.9×10^5 to 4.9×10^6. The figure shows some collapse of the data when $Nu_{av}/Re_\phi^{0.8}$ is plotted against the Rossby number ($\varepsilon = U_{in}/\Omega a$). The peak in $Nu_{av}/Re_\phi^{0.8}$ (at ε about equal to 2) corresponds to conditions for which vortex breakdown has been observed in isothermal flow and a minimum in the cavity tangential velocity has been measured in heated flow (Owen and Pincombe 1979; Farthing et al. 1990a). The collapse of the data using the parameter $Nu_{av}/Re_\phi^{0.8}$ suggests that turbulent flow dominated the heat transfer. It should be noted, however, that this is a complex flow, and different mechanisms may dominate in different regions of the cavity and different parameter ranges.

At lower values of the Rossby number, it is expected that the 3-D nature of the flow due to the vortex breakdown and buoyancy effects as observed experimentally are important. Prediction of these is beyond the scope of this study. However,

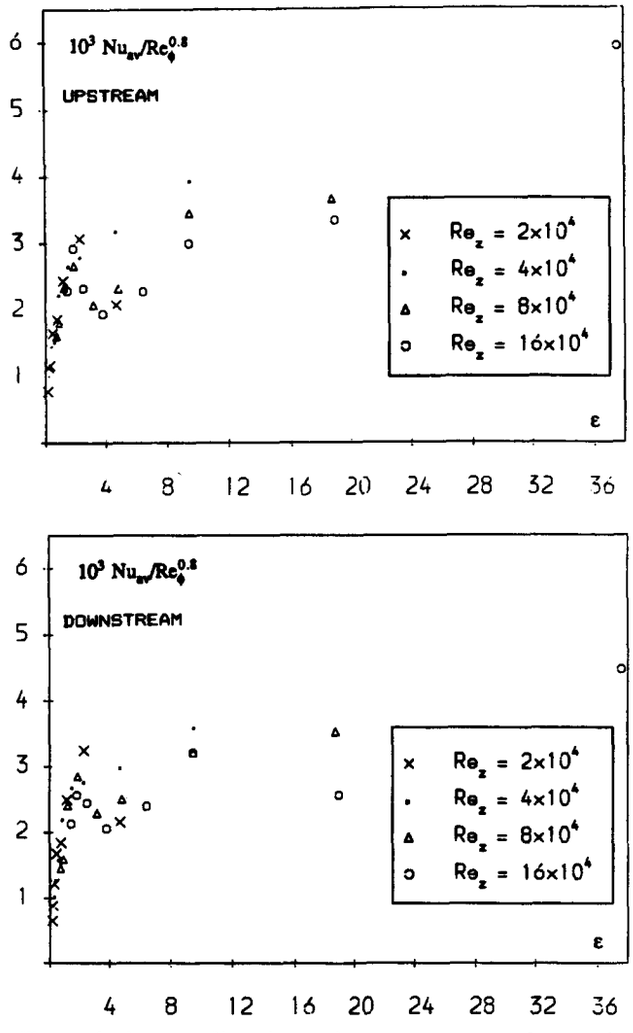

Figure 4 Average Nusselt number measurements for rotating cavity with axial throughflow. Farthing et al. (1990a)

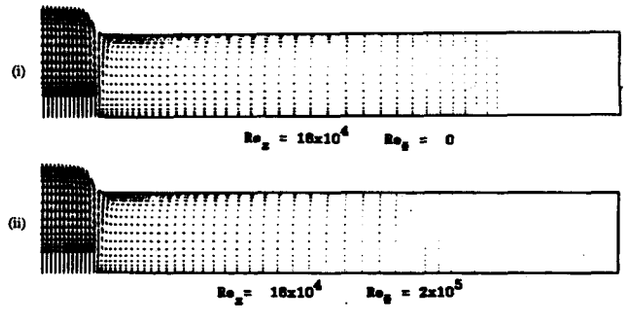

Figure 5 Predicted flowfield for a cavity with axial throughflow

as the Rossby number increases, rotational effects diminish, and a point may be reached where the recirculation induced in the cavity by the central axial jet dominates. This limiting condition is considered below.

Figure 5 shows velocity vector plots for the two cases calculated using the k-ε/1-eqn turbulent model. The throughflow rate in both cases is the maximum studied experimentally ($Re_z = 16 \times 10^4$), and the rotational Reynolds numbers are 0 and 2×10^5, corresponding to Rossby numbers of infinity and 35.6. It can be seen that a toroidal vortex is predicted in the inner part of the cavity and that the extent of this vortex is reduced in the rotating case.

Heat transfer predictions from the k-ε/1-eqn model are shown and compared with measurements in Figures 6 and 7. In the calculations a disc temperature distribution for the radial outflow case in the previous section was used, this being similar to that measured by Farthing et al. Calculations using the ML model were made for this example but are not shown in the figures. Not surprisingly, given the limitations of this model, the ML results showed very low levels of cavity flow and heat transfer. Considerable discrepancies are apparent between the measurements and k-ε/1-eqn calculations. These might have been expected due to uncertainty with inlet and temperature boundary conditions, measurement inaccuracy, the 3-D effects mentioned above, and shortcomings in the turbulence model

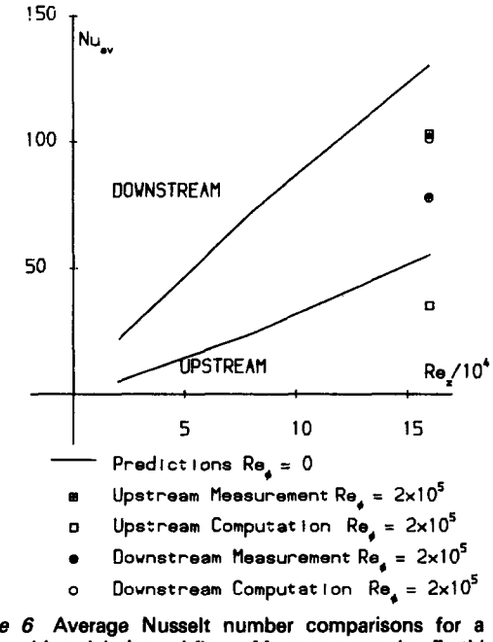

Figure 6 Average Nusselt number comparisons for a rotating cavity with axial throughflow. Measurements by Farthing et al. (1990a)

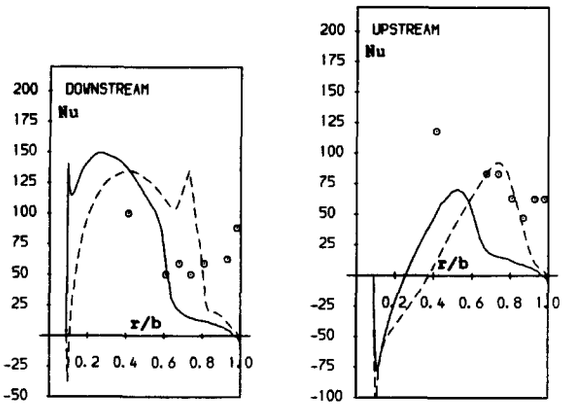

Figure 7 Local Nusselt number comparisons for a cavity with axial throughflow at $Re_z = 1.6 \times 10^4$ ———: k-ε/1-eqn, $Re_\phi = 2 \times 10^5$; – – – –: k-ε/1-eqn, $Re_\phi = 0$; ○: Measurement $Re_\phi = 2 \times 10^5$, Farthing et al. (1990a)

for calculating flow at a pipe expansion (see Yap 1987). Note also that the calculations do indicate some influences of rotation for $\varepsilon = 35.6$. Nevertheless, some important deductions may be drawn from the comparison. At high flow rates, the magnitudes of the calculated and measured mean Nusselt numbers are comparable, indicating that the induced recirculation can at least be a significant influence on heat transfer for these conditions. This is especially so in the inner part of the cavity for which only limited instrumentation was available in the experiments. Considering the various uncertainties, it would not be appropriate to draw any firm conclusions regarding turbulence modeling, but it may be noted that the transport models offer a much better prospect than the mixing-length approach.

A variety of rotating cavities with axial throughflow occur in engines, but generally these have a higher ratio of inner to outer radius than that considered above and have a central differentially rotating shaft. Temperature distributions also vary considerably during a flight cycle, so it is possible that under certain engine conditions the buoyancy and vortex breakdown phenomena reported by Farthing et al. do not occur and an axisymmetric analysis of the type given here may prove useful. Clearly, further research is needed to delineate the various regimes and produce validated mathematical models.

6. A rotor-stator system with radial outflow

Bunker et al. (1990a, 1990b) and Bunker (1990) applied a liquid crystal technique to measure heat transfer in a rotor-stator system similar to that in Figure 1(iii). Although results were obtained for various radial locations of the inlet jet, only the axisymmetric case with the jet at the hub is considered here. The outer radius of the cavity, b, is 104 mm, the rotor radius (r_o) is 100 mm, the axial spacing, s, is 15 mm and the inlet jet radius is 2.5 mm in the example below. In the calculations, uniform properties of the flow were assumed at conditions appropriate to the experiment and frictional heating effects were neglected.

Velocity vectors and tangential velocity contours of tangential velocity for a rotational Reynolds number of 5.4×10^5 (the upper end of the experimental range) and a flow rate corresponding to $C_w = 1{,}450$ are given in Figure 8. These were obtained using the k-ε/1-eqn model. The predicted flow is seen to be dominated by the impinging inlet jet at the center of the cavity. (This is not surprising, since the inlet axial velocity is about 1.5 times the disc tip speed Ωr_o.) Towards the outer part of the cavity, rotational effects dominate, with the characteristic disc boundary layers and axial flow from the stator to the rotor across the core region. A change in direction of the axial velocity across the core occurs in the region of $r/r_o = 0.7$, as the recirculation induced by the inlet and wall jets gives way to that of the rotationally driven flow.

In the experiments the inlet temperature was approximately constant for a particular test at 323 to 353 K, and the discs and shroud were initially at a uniform temperature of about 293 K. Surface heat transfer distributions were deduced from the time taken for points on the surfaces to reach the liquid-crystal detection temperature of 312 K. Time scales are such that it is reasonable to neglect transient effects in the flow, but the change in surface temperature distribution during the test may well influence the measured Nusselt numbers. This will be most important in regions of relatively low heat transfer where the time taken to reach the detection temperature is longest. A further complication is the possibility of air from outside the cavity being drawn in through the outlet. This might be expected to reduce the heat transfer in the experiment, particularly in the outer part of the cavity. From an elementary model of ingress calibrated against the available data for similar configurations (Chew 1991), an ingress level of 80 percent of the inlet flow has been estimated, though a good deal of uncertainty must be recognized.

Heat transfer measurements for the rotor and stator discs are compared with prediction assuming uniform cavity surface temperature using the k-ε/1-eqn and ML models in Figure 9, Case (i). On the rotor, the ML results are in remarkably good agreement with the measurements for $r/r_o < 0.8$, which includes the impingement-dominated heat transfer region. However, on the stator, the mixing length gives unrealistically very low heat transfer rates. The k-ε/1-eqn results might be regarded as reasonable on the rotor, but despite some improvement over the ML model they are again too low on the stator. The sensitivity of the Nusselt numbers to surface temperature distribution may be gauged by comparing the Figure 9 calculations for Case (i) with those for Case (ii) for a uniform wall heat-flux boundary condition. Further calculations, which are not shown, confirmed the significant effect of temperature distribution and also showed that ingress could also modify the results. Despite the uncertainties, it is considered reasonable to conclude that the main area of discrepancy between the predictions and measurement is on the stator. The k-ε/1-eqn model does better than the ML model here but shows clear differences from the measurements. In particular, the calculations fail to reproduce the measured maximum in Nu at $r/b = 0.6$.

Although the experimental data may not be ideal for the purposes of evaluating turbulence models, it may be noted that in applying these methods to engine conditions an engineer may well face similar uncertainties regarding thermal boundary conditions and ingress. Thus the level of agreement shown above is perhaps representative of the quality of prediction that

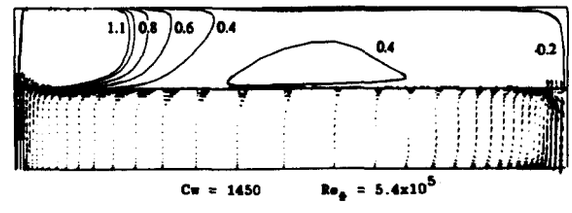

Figure 8 Predicted velocity vectors and $W/\Omega r$ contours for a rotor-stator system with radial outflow. Velocity vectors scaled by $\max[(r/a)^{1/2}, 1]$ and axial velocity scaled by $\max(r/a, 1)$

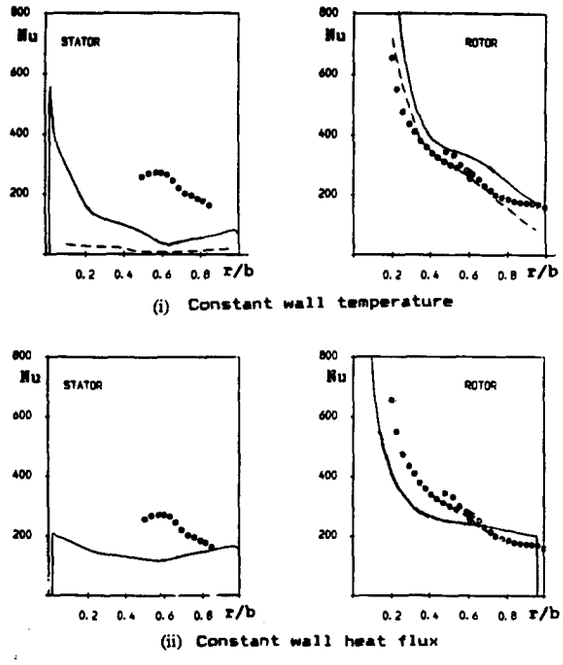

Figure 9 Local Nusselt number comparisons for a rotor-stator system with radial outflow. $C_w = 1{,}450$ and $Re_\phi = 5.4 \times 10^5$. ———: k-ε/1-eqn; – – – –: Mixing length; ○: Measurements, Bunker et al. (1990b) and Bunker (1990)

would be obtained in engineering calculations. A more stringent test of the predictive capability would have been to calculate the transient development of the temperature field during the experiment. This is plausible for this example but would require significantly more effort.

7. Conclusions

Prediction of convective heat transfer in rotating disc cavities representative of gas-turbine engine configurations has been considered. Calculations from axisymmetric, finite-difference programs using various turbulence models were compared with other workers' recent measurements for three different model problems. These problems involve heat transfer regions dominated by Ekman-type boundary layers, impingement, and recirculation zones. It is concluded that, used with care, the present methods are suitable for engineering calculation in certain classes of disc cavity flows. A two-layer k-ε/1-eqn turbulence model was found to perform reasonably well, although areas where further turbulence modeling refinement may be necessary are identified. Further experimental and numerical research is needed to extend the parameter range for methods validation and to delineate the various heat transfer regimes that may occur.

For a rotating cavity with radial outflow, it was found that under rotationally dominated conditions the mixing-length model and the k-ε/1-eqn and k-ε/ML1 two-layer models gave reasonable agreement with experiment. For conditions where rotation was relatively weak, the mixing-length model performed badly, while performance of the two-layer models could again be said to be reasonable. From these comparisons and for consistency within a wide evaluation of turbulence models, the k-ε/1-eqn model was selected as being the preferred two-layer approach.

Comparison with heat transfer data for a rotor-stator cavity with an inlet jet at the hub has shown reasonable performance of the mixing-length and k-ε/1-eqn model for the rotating disc, which includes regions where either the jet impingement or rotation dominate. On the stationary disc, the two-layer model performs significantly better than the mixing-length model, but still shows notable discrepancies with the data. The numerical model has been used to show the effects of thermal boundary conditions and ingestion at the rim for this example.

Examination of measurements for a rotating cavity with a central axial throughflow has clarified the interpretation of the heat transfer data. At low Rossby numbers, 3-D and buoyancy effects are expected to be important, so the axisymmetric assumption used here is invalid. However, at high Rossby numbers, the heat transfer may be dominated by the recirculation in the cavity generated by the central throughflow. The general level of heat transfer predicted using the k-ε/1-eqn model for this extreme case is consistent with measurements, although considerable uncertainty remains. The suitability of the two-layer model for this flow has not been properly demonstrated for this case, but it is clearly preferable to the mixing-length model. Of the three rotating disc configurations studies, this is the least well understood and the most challenging for mathematical models. Considerable further work is likely to be required before a mathematical model can be recommended for engineering predictions with any confidence.

Acknowledgments

Funding for this work from the Ministry of Defence and Rolls-Royce plc is gratefully acknowledged. We would also like to thank Dr C. M. Vaughan for assistance with some of the computations, Dr. C. A. Long and Professor J. M. Owen for providing tabulated data, and Professor B. E. Launder for helpful comments. The manuscript has been prepared by Mrs I. Bowker and Mrs J. Buckley with their appreciated care.

References

Bunker, R. S. 1990. Measurement of local heat transfer on rotating and stationary surfaces for application to disc-cavity cooling in turbine engines — Summary Report. ITS, University of Karlsruhe, Germany

Bunker, R. S., Metzger, D. E., and Wittig, S. 1990a. Local heat transfer in turbine disc-cavities, Pt. 1: Rotor-stator cooling with hub injection of coolant. ASME, 90-GT-25, Gas Turbine and Aeroengine Congress, June 1990, Brussels, Belgium

Bunker, R. S., Metzger, D. E., and Wittig, S. 1990b. Local heat transfer in turbine disc-cavities, Pt. 2: Rotor cooling with radial location injection of coolant. ASME 90-GT-26, Gas Turbine and Aeroengine Congress, June 1990, Brussels, Belgium

Chang, C. J., Humphrey, J. A. C., and Greif, R. 1990. Calculation of turbulent convection between corotating discs in axisymmetric enclosures. *Int. J. Heat Mass Transfer*, **33**, 2701–2720

Chew, J. W. 1985. Prediction of flow in a rotating cavity with radial outflow using a mixing length turbulence model. *Proc. Int. Conf. on Numer. Meths. in Laminar and Turbulent Flows*, Pineridge Press, Swansea, UK, 318–329

Chew, J. W. and Rogers, R. H. 1988. An integral method for the calculation of turbulent forced convection in a rotating cavity with radial outflow. *Int. J. Heat Fluid Flow*, **9**, 37–48

Chew, J. W. and Vaughan, C. M. 1988. Numerical predictions for the flow induced by an enclosed rotating cavity. ASME, 88-GT-127, Gas Turbine and Aeroengines Congress, 1988, Amsterdam

Chew, J. W. 1990. Prediction of rotating disc flow and heat transfer in gas turbine engines. *Proc. 3rd Int. Symp. Transport Phenomena and Dynamics of Rotating Machinery*, Honolulu

Chew, J. W. 1991. A theoretical study of ingress for shrouded rotating disc systems with radial outflow. *AMSE J. Turbomachinery*, **113**, 91–97

Daily, J. W. and Nece, R. E. 1960. Chamber dimension effects on induced flow and frictional resistance of enclosed rotating discs. *ASME J. Basic Eng.* **82**, 217

Daily J. W., Ernst, W. D., and Asbedian, V. 1964. Enclosed rotating discs with superposed throughflow; mean steady and periodic unsteady characteristics of induced flow, Report No. 64, Hydrodynamic Lab., MIT64, MIT, Cambridge, MA

Ekman, V. M. 1905. On the influence of the earth's rotation on ocean-currents. *Ark. Mat. Asta. Fys.*, **30**, 365–375

Farthing, P. R., Long, C. A., Owen, J. M., and Pincombe, J. R. 1990a. Rotating cavity with axial throughflow of cooling air: Heat transfer. ASME, 90-GT-16, Gas Turbine and Aeroengine Congress, June 1990, Brussels, Belgium

Farthing, P. R., Long, C. A., Owen, J. M., and Pincombe, J. R. 1990b. Rotating cavity with axial throughflow of cooling air: Flow structure. ASME, 90-GT-17, Gas Turbine and Aeroengine Congress, June 1990, Brussels, Belgium

Iacovides, H. and Theofanopoulos, I. P. 1991. Turbulence modelling of axisymmetric flow inside rotating cavities. *Int. J. Heat Fluid Flow*, **12**, 2

Jones, W. P. and Launder, B. E. 1972. Prediction of laminarization with a two equation model of turbulence. *Int. J. Heat Mass Transfer*, **15**, 301

Koosinlin, M. L., Launder, B. E., and Sharma, B. I. 1974. Prediction of momentum heat and mass transfer in swirling turbulent boundary layers. *J. Heat Transfer*, **98**, 204

Morse, A. P. 1987. Numerical prediction of turbulent flow in rotating cavities. ASME, 87-GT-74, Gas Turbine Conf. and Ex., Anaheim, CA

Morse, A. P. and Ong, C. L. 1990. Computation of heat transfer in rotating cavities using a two-equation model of turbulence. ASME, 90-GT-135, Gas Turbine and Aeroengine Congress, Brussels, Belgium

Northrop, A. 1984. Heat transfer in a cylindrical rotating cavity. D.Phil. Thesis, University of Sussex, UK

Northrop, A. and Owen, J. M. 1988. Heat transfer measurements in rotating-disc systems. Pt 2: The rotating cavity with a radial outflow of cooling air. *Int. J. Heat Fluid Flow*, **9** (1), 27

Ong, C. L. and Owen, J. M. 1989. Prediction of heat transfer in a rotating cavity with radial outflow. Paper No. 89-GT-286, 34th ASME Int. Gas Turbine Conf., Toronto

Owen, J. M. and Pincombe, J. R. 1979. Vortex breakdown in a rotating cylindrical cavity. *J. Fluid Mech.*, **90**, 109–129

Owen, J. M., Pincombe, J. R. and Rogers, R. H. 1985. Source-sink flow inside a rotating cylindrical cavity. *J. Fluid Mech.*, **155**, 233

Rodi, W. 1990. Some current approaches in turbulence modelling. AGARD Technical Meeting on Appraisal of the Suitability of Turbulence Models in Flow Calculations, Friedrichshafen

Roscoe, D. V., Buggela, R. C., Foster, J. A., and McDonald, H. 1988. A numerical investigation of fluid flow for disc pumping applications. ASME, 88-GT-299, Gas Turbine and Aeroengine Congress, Amsterdam

Subburaman, M. R., Hadid, A. H. and McConnaughey, P. K. 1990. Numerical evaluation of single central jet for turbine disc cooling. *Proc. 3rd Int. Symp. Transport Phenomena and Dynamics of Rotating Machinery*, Honolulu

Van Driest, E. R. 1956. On turbulent flow near a wall. *J. Aero Soc.*, **23**, 1007

Vaughan, C. M., Gilham, S., and Chew, J. W. 1989. Numerical solutions of rotating disc flows using a non-linear multigrid algorithm. *Proc. 6th Int. Conf. Numer. Meth. Laminar and Turbulent Flow*, Swansea, UK

Wolfshtein, M. 1969. The velocity and temperature distribution in one-dimensional flow with turbulence augmentation and pressure gradient. *Int. J. Heat Mass Transfer*, **12**, 301

Yap, C. R. 1987. Turbulent heat and momentum transfer in recirculating and impinging flows. Ph.D. thesis, Faculty of Technology, University of Manchester, UK